optica

Selective two-photon collagen crosslinking *in situ* measured by Brillouin microscopy

Sheldon J. J. Kwok,[1,2,†] Ivan A. Kuznetsov,[2,3,†] Moonseok Kim,[2] Myunghwan Choi,[2,4] Giuliano Scarcelli,[2,5] and Seok Hyun Yun[1,2,*]

[1]Harvard-MIT Division of Health Sciences and Technology, 77 Massachusetts Avenue, Cambridge, Massachusetts 02139, USA
[2]Wellman Center for Photomedicine, Massachusetts General Hospital, 50 Blossom Street, Boston, Massachusetts 02114, USA
[3]Department of Biomedical Engineering, Johns Hopkins University, 3400 North Charles Street, Baltimore, Maryland 21218, USA
[4]Department of Biomedical Engineering, Sungkyunkwan University and Center for Neuroscience and Imaging Research, Institute for Basic Science (IBS), Suwon 16419, South Korea
[5]Fischell Department of Bioengineering, University of Maryland, College Park, Maryland 20742, USA
*Corresponding author: syun@hms.harvard.edu

Received 25 January 2016; revised 14 March 2016; accepted 18 March 2016 (Doc. ID 258116); published 4 May 2016

Two-photon polymerization has enabled the precise microfabrication of three-dimensional structures with applications spanning from photonic microdevices, drug delivery systems, and cellular scaffolds. We present two-photon collagen crosslinking (2P-CXL) of intact corneal tissue using riboflavin and femtosecond laser irradiation. The collagen fiber orientations and photobleaching were characterized by second harmonic generation and two-photon fluorescence imaging, respectively. The measurement of local changes in longitudinal mechanical moduli with confocal Brillouin microscopy enabled the visualization of the cross-linked pattern without the perturbation of the surrounding non-irradiated regions. 2P-CXL-induced stiffening was comparable to that achieved with conventional one-photon CXL. Our results demonstrate the ability to selectively stiffen biological tissue *in situ* at high spatial resolution, with broad implications in ophthalmology, laser surgery, and tissue engineering.

OCIS codes: (190.4180) Multiphoton processes; (180.0180) Microscopy; (290.0290) Scattering; (170.6935) Tissue characterization; (170.4470) Ophthalmology.

http://dx.doi.org/10.1364/OPTICA.3.000469

Light-induced polymerization and crosslinking are widely used methods for the fabrication and processing of polymeric materials, with applications ranging from manufacturing, photolithography, and tissue engineering. In most cases, the photochemical mechanism involves light absorption by a photosensitive compound, leading to the generation of free radicals that promote the polymerization of monomers or the crosslinking of polymers [1]. These methods are increasingly common for clinical applications since they enable the fabrication and manipulation of biomaterials *in situ*, including curing of dental composites [2] and photocrosslinking of polymer implants for regenerative medicine applications [3]. Some biological tissues, such as the cornea, are composed of intricate collagen fiber networks that can degrade due to diseases, but crosslinking can restore their natural biomechanical properties and functions [4,5]. Corneal ectatic disorders, for example, caused by the weakening of the corneal stroma, is effectively treated with photochemical crosslinking using riboflavin and ultraviolet A (UVA) light to strengthen corneal tissue [6].

While most applications rely on single-photon absorption (typically UV light), two-photon absorption-mediated processes using a near-infrared (NIR) femtosecond laser offers far superior spatial resolution that is confined to the focal volume. Two-photon polymerization is the basis for a liquid-based three-dimensional printing process [7] in which either unpolymerized regions (negative photoresist) or polymerized regions (positive photoresist) are washed away with a developing solvent, leaving only the fabricated structure. This technique has been used to fabricate micro-optic components [8], and hydrogel-based cellular scaffolds [9]. Two-photon crosslinking of proteins in solution has also been reported, including bovine serum albumin [10] and collagen [11]. However, the use of two-photon processes for the precise, internal modification of soft condensed materials, such as biological tissues, has not been reported. A major challenge has been a lack of appropriate tools to monitor and characterize crosslinked regions nondestructively. One study attempting two-photon collagen crosslinking (2P-CXL) in corneal tissue reported changes in collagen second harmonic generation (SHG), but with no evidence of crosslinking [12]. Two other studies have shown the feasibility of 2P-CXL for the stiffening of biomaterials, including artificial cardiac tissue [13] and collagen hydrogels [14]. However, the depth-selective ability of 2P-CXL was not demonstrated, since conventional indentation testing requires physical contact with the sample, limiting the measurements to only surface properties.

In this Letter, we demonstrate spatially selective 2P-CXL of intact tissue for the first time to our knowledge. We use femtosecond laser pulses and riboflavin, a clinically approved photosensitizer, to crosslink a small volume within animal corneas. We characterize collagen crosslinking non-invasively *in situ* with multiphoton imaging and after the procedure with confocal

Brillouin microscopy. Our results demonstrate the ability to alter the microstructure and mechanical modulus locally in the cornea by 2P-CXL with microscopic resolution and illustrate the unique advantage of Brillouin microscopy in evaluating 2P-CXL induced changes nondestructively.

Before characterizing 2P-CXL, we first characterized standard one-photon CXL (1P-CXL) with riboflavin and UV light (365 nm, 3 mW/cm^2, 30 min). We imaged riboflavin fluorescence and backscattered SHG from collagen fibers in excised, de-epithelialized bovine corneas (see Supplement 1). We used a home-built two-photon microscope with a 1.0 NA water immersion objective lens (Fig. 1). Our light source consisted of a mode-locked Ti:Sapphire laser delivering 810 nm light at 150 fs pulses and an 80 MHz repetition rate.

Application of a 0.1% riboflavin, 10% dextran solution to the excised corneas for 30 min caused significant dehydration, resulting in a decrease in corneal thickness from 713 ± 37 μm before dye application to 473 ± 41 μm after staining, which was unchanged at 485 ± 19 μm following CXL (Fig. 2). Fluorescence imaging revealed riboflavin dye penetration over 300 μm below the cornea surface, which was bleached significantly following 1P-CXL. The mean SHG intensity increased following dye application and CXL but was highly variable. The changes in SHG could be attributed to the decreased attenuation by riboflavin absorption, as well as the alteration of collagen fiber distribution, structure and morphology; the latter can significantly affect the intensity and angular distribution of SHG [15]. To explore this further, we next investigated whether the collagen morphology obtained from SHG imaging could be a suitable metric for CXL.

The two-dimensional fast Fourier transform (2D-FFT) of the SHG image can be used to quantify the fiber orientation [16,17]. Following filtering to suppress background autofluorescence (Fig. S1), the magnitude of the 2D-FFT gives the integrated power spectrum, which can be interpreted as the number of fibers as a function of the orientation angle [17]. The data was fit to a bimodal von Mises distribution, from which the variance specifies the alignment of the fibers. We found that the orientation distribution of the collagen fibers increases markedly with the application of the riboflavin-dextran solution, such that the fiber orientations are essentially randomly distributed [Fig. 2(c) and Fig. S2]. Subsequent 1P-CXL did not cause any appreciable change to the distribution of the fiber orientations. Our results agree with qualitative observations made previously [18,19], but it is unclear whether any changes in fiber orientation are sustained with corneal rehydration [20].

To determine the parameters needed for 2P-CXL, we first measured the two-photon photobleaching kinetics of riboflavin

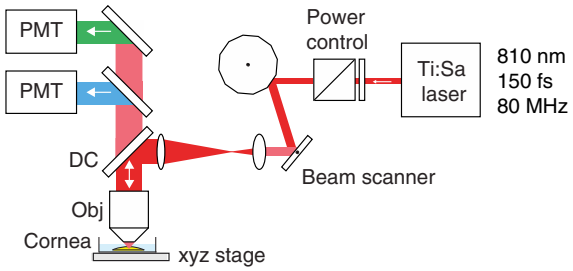

Fig. 1. Home-built two-photon microscope. The cornea sample was compressed with a coverslip. The SHG (blue, 400 to 410 nm) and fluorescence (green, 485 to 555 nm) were collected through the appropriate dichroic mirrors and filters by separate photomultiplier tubes.

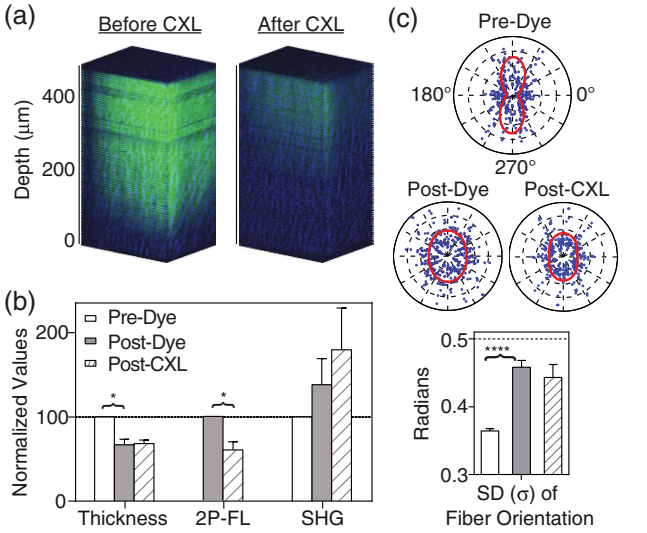

Fig. 2. Assessment of 1P-CXL with multiphoton imaging. (a) Reconstructed depth profile of riboflavin-soaked corneas before and after CXL. Green: riboflavin fluorescence, Blue: backscattered collagen SHG. (b) Summary of changes, with mean ± std. error reported. *, $p < 0.05$. (c) Top: distribution of collagen fiber orientations determined by 2D-FFT. Red: fitting to von Mises distribution. Bottom: standard deviation (σ) of the fiber orientation. A uniform fiber distribution is defined to have a σ of 0.5 radians (dotted line). ****, $p < 0.0001$.

in solution as a function of the incident laser power from 104 to 230 mW. The power dependence of the bleaching rate was found to be nearly quadratic ($n = 1.9 \pm 0.3$), indicating a two-photon absorption mechanism [Fig. 3(a)]. Next, we scanned a laser beam at 200 mW over a cross-sectional plane 50 μm below the cornea surface for 20 min (6.6 ms per focal spot) and measured both photobleaching and SHG. We observed a small yet significant 4.3 ± 1.6% decrease in fluorescence ($p < 0.01$) [Fig. 3(b)]. Compared to riboflavin bleaching in solution, photobleaching in tissue is much slower, considering the light scattering and rapid diffusion of non-bleached riboflavin (~40 μm^2/s) [21]. Both the mean SHG intensity and the collagen fiber orientation were unchanged with 2P-CXL [$p > 0.05$, Fig. 3(b)]. The insensitivity of SHG to 2P-CXL of a single plane underscores the need for a more specific metric for evaluating crosslinking.

Finally, we compared the laser parameters used for conventional 1P-CXL with 2P-CXL, assuming that an equal number of molecular excitations is needed to elicit the same crosslinking effect (see Supplement 1). We found that at an average power of 100 mW, 2P-CXL of our (290 × 480) μm^2 scanning area would require ~2.1×10^4 J/cm^2. In subsequent samples characterized with Brillouin microscopy, 2P-CXL was performed on riboflavin-stained corneas at 104 mW with scanning times of 10 min per plane (~4.3×10^4 J/cm^2), accounting for losses due to optical aberration and light scattering. While no discernable tissue damage was observed at 207 mW for up to 20 min, irradiation with 312 mW for 5 min resulted in tissue damage, likely due to nonlinear photochemical and photothermal effects causing low-density plasma formation [22] [Fig. 3(c)].

Unlike measurements of riboflavin fluorescence and collagen SHG, Brillouin microscopy contrast is directly dependent on the local hydromechanical properties of the tissue. Brillouin microscopy has been used to characterize normal and keratoconic

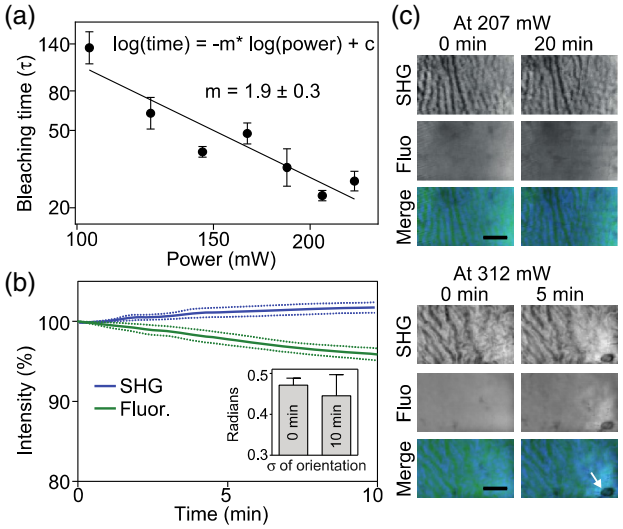

Fig. 3. Determination of laser parameters for 2P-CXL. (a) Two-photon bleaching time constant (1/e) in seconds as a function of the incident laser power (mW). Mean ± std. error are reported. Black line is linear fit to ln(τ) vs. ln(power). (b) Changes in SHG and fluorescence with 2P-CXL. Mean (solid line) ± std. error (dotted line) are reported. Inset: change in the standard deviation (σ) of fiber orientations. (c) There is no tissue damage with 20 min irradiation at 207 mW, but there is significant photodamage with 5 min irradiation at 312 mW (white arrow). SHG (blue) and fluorescence (green) channels are shown. Scale bar: 50 μm.

corneas *in vivo* [23], as well as the effects of 1P-CXL *ex vivo* [24]. This technique relies on the scattering of photons by spontaneous acoustic waves, which are sensitive to changes in the compressibility of the local microenvironment, modulus of collagen fibers, and the crosslink density of the network [Fig. 4(a)]. The resulting shift in optical frequency is detected using a high-resolution spectrometer. Using a previously described confocal Brillouin microscope [25] [Fig. 4(b)], we imaged a cornea immediately following 2P-CXL-induced stiffening of an arbitrary three-dimensional region centered around 50 μm below the surface (10 successive planes, 3 μm apart). The distribution of riboflavin over these depths is nearly uniform (Fig. S3).

Scanning large areas of the cornea, we readily identified a region with significantly increased Brillouin frequency shifts, indicating local stiffening (Fig. S4). Focusing on the stiffened region, we then took x–z and x–y scans, which were reconstructed as a three-dimensional volume (Fig. 5 and Visualization 1). A rectangular volume spanning approximately $(205 \times 325 \times 50)\mu m^3$ was found to be significantly stiffer than the surrounding regions [Fig. 5(c)]. These dimensions compare to a volume of $(290 \times 480 \times 30)\mu m^3$ that was irradiated with our two-photon microscope. While the total volume of the 2P-CXL region is nearly conserved, the discrepancy in area and thickness was attributed to flattening of the sample with a coverslip during 2P-CXL, which was required for use with our high NA, water immersion objective. In contrast, with Brillouin microscopy, the cornea was imaged in its natural condition without artifacts caused by coverslip compression. Distortion from a rectangular shape can be attributed to optical aberrations leading to a reduced intensity at the periphery of the scanning area in the two-photon microscope.

The mean Brillouin shift over the anterior 300 μm of the untreated cornea was 8.15 ± 0.04 GHz, in agreement with

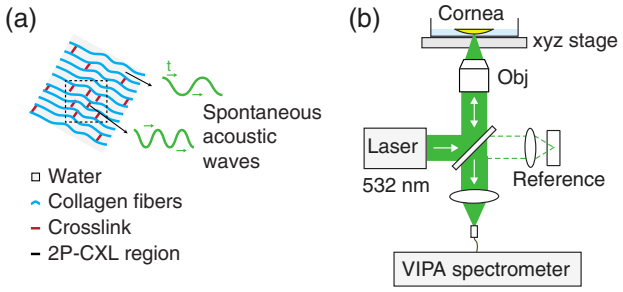

Fig. 4. Brillouin microscopy. (a) Brillouin scattering is due to interaction of photons and spontaneous acoustic waves. For the 2P-CXL region, the acoustic velocity is higher for a given phase-matched phonon wavelength. (b) Confocal Brillouin microscope connected to a two-stage, apodized, virtually imaged phased array spectrometer.

previous *ex vivo* studies measured at the same wavelength of 532 nm [24,26]. The depth profile of the 2P-CXL region and the surrounding non-irradiated region is plotted in Fig. 6(a). Over depths of 30 to 80 μm below the surface, 2P-CXL increased Brillouin frequency shifts by 0.3 to 0.6 GHz. This corresponds to an estimated increase of 0.2 to 0.4 GPa in the longitudinal modulus (see Supplement 1). The relative Brillouin shift across the irradiated volume was fitted to a Gaussian function, giving a peak of 548 ± 7 MHz at a depth of 55.7 ± 0.3 μm and an FWHM of 48.7 ± 0.7 μm [Fig. 6(b)]. This gradual change in the Brillouin shift is largely due to the limited axial resolution of the 0.3-NA objective lens used. The degree of stiffening achieved by 2P-CXL is comparable to a ~0.5 GHz increase previously measured in the anterior cornea with conventional 1P-CXL [24]. Notably, 1P-CXL causes significant stiffening over nearly the entire stromal depth over >500 μm [Fig. 1(a)], while 2P-CXL-induced stiffening can be localized to target depths [Fig. 5(b)].

In summary, we have demonstrated three-dimensional selective crosslinking in corneal tissue. Our technique involves (1) *in situ* 2P-CXL of an arbitrary three-dimensional structure, and (2) verification and characterization with confocal Brillouin microscopy. Compared to conventional procedures for evaluating 2P-CXL-induced stiffening, Brillouin microscopy does not require

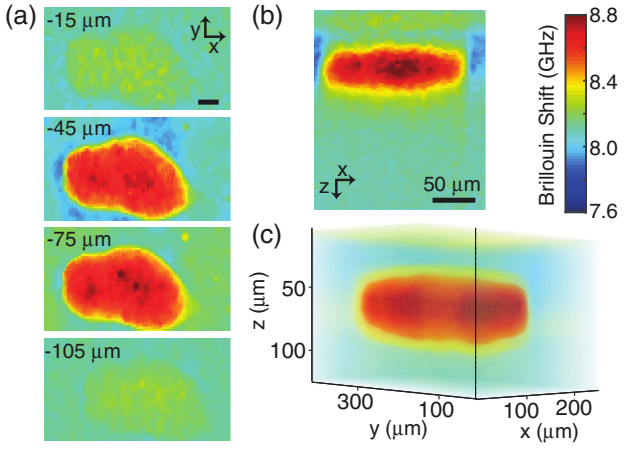

Fig. 5. Brillouin microscopy of a 2P-CXL-treated cornea. (a) x–y images of the 2P-CXL region, at 15, 45, 75, and 105 μm below the cornea surface. Scale bar: 50 μm. b) x–z image, where top refers to the surface of the cornea. (c) Three-dimensional view of the 2P-CXL region reconstructed and interpolated from thirteen x–y images (selected images shown in a) at 10 μm intervals in z.

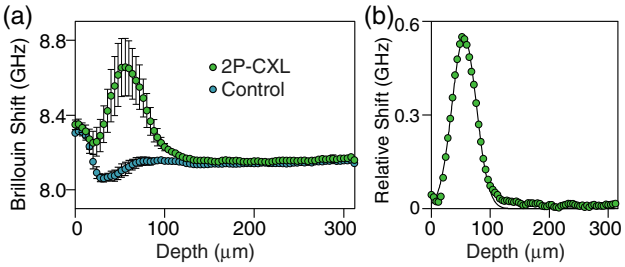

Fig. 6. Quantification of 2P-CXL-induced stiffening. (a) Mean (± st. dev.) Brillouin shift of the crosslinked and non-irradiated regions of the cornea as a function of depth. (b) Relative Brillouin shift obtained from subtracting the profiles in (a). Fit to Gaussian function ($R^2 = 0.99$).

perturbation of the surrounding non-crosslinked regions. Other non-invasive approaches for measuring tissue elasticity include elastographic techniques based on ultrasound [27] or magnetic resonance imaging [28], but at typical spatial resolutions of hundreds of microns to several millimeters, respectively. An emerging technique is optical coherence elastography, which can be used to extract viscoelastic properties by optical measurement of mechanically induced tissue deformations [29].

Our current technique is limited by the long irradiation times needed for 2P-CXL, about 1 h per mm^2. Faster 2P-CXL could be achieved by using wide-field two-photon microscopy techniques such as light sheet or Bessel beam plane illumination [30,31]. Although riboflavin was chosen for direct comparison with conventional corneal CXL, it has a relatively low two-photon absorption cross-section at 810 nm (<1 GM), which can be enhanced by a factor of ~2–3 by excitation at 760 nm [14,32]. More efficient two-photon photosensitizers are also in development [33]. Increasing the peak irradiance by the use of shorter pulse width or lower repetition rate lasers could shorten 2P-CXL times, but careful selection of laser parameters is needed to avoid nonlinear photodamage [Fig. 3(c)]. Another challenge is the acquisition time needed for Brillouin microscopy, typically over 30 min per image in this work. The exposure time could be decreased with a better signal-to-noise ratio, such as by improving the filtering of background Rayleigh scattering [34]. Future development of a combined two-photon and Brillouin imaging setup would enable the real-time measurement and feedback control of 2P-CXL-induced stiffening.

Our current 2P-CXL technique can be employed for applications involving micron-scale target regions, such as microfabrication and patterning, as well as precise laser surgeries. Nonlinear excitation permits three-dimensional control of crosslinking, while the use of NIR light enables deep tissue penetration. 2P-CXL can be readily applied in ophthalmology, such as for treatment of thin ectatic corneas (<400 μm) [6], corneal flap bonding post-LASIK surgery, and the selective modulation of corneal curvature for refractive error correction.

Funding. National Institutes of Health (NIH) (P41-EB015903, R01-EY025454, UL1-RR025758); National Science Foundation (NSF) (CBET-0853773, EEC-1358296).

Acknowledgment. We thank Peng Shao and Sebastien Besner for useful discussions.

†These authors contributed equally.

See Supplement 1 for supporting content.

REFERENCES

1. J. P. Fisher, D. Dean, P. S. Engel, and A. G. Mikos, Annu. Rev. Mater. Res. **31**, 171 (2001).
2. I. Sideridou, V. Tserki, and G. Papanastasiou, Biomaterials **23**, 1819 (2002).
3. A. T. Hillel, S. Unterman, Z. Nahas, B. Reid, J. M. Coburn, J. Axelman, J. J. Chae, Q. Guo, R. Trow, A. Thomas, Z. Hou, S. Lichtsteiner, D. Sutton, C. Matheson, P. Walker, N. David, S. Mori, J. M. Taube, and J. H. Elisseeff, Sci. Transl. Med. **3**, 93ra67 (2011).
4. K. M. Meek, S. J. Tuft, Y. Huang, P. S. Gill, S. Hayes, R. H. Newton, and A. J. Bron, Investig. Opthalmology Vis. Sci. **46**, 1948 (2005).
5. G. Fessel, C. Gerber, and J. G. Snedeker, J. Shoulder Elbow Surg. **21**, 209 (2012).
6. N. Sorkin and D. Varssano, Ophthalmologica **232**, 10 (2014).
7. J.-F. Xing, M.-L. Zheng, and X.-M. Duan, Chem. Soc. Rev. **44**, 5031 (2015).
8. S. A. Rinne, F. García-Santamaría, and P. V. Braun, Nat. Photonics **2**, 52 (2007).
9. J. Torgersen, X. H. Qin, Z. Li, A. Ovsianikov, R. Liska, and J. Stampfl, Adv. Funct. Mater. **23**, 4542 (2013).
10. D. Serien and S. Takeuchi, Appl. Phys. Lett. **107**, 013702 (2015).
11. A. Bell, M. Kofron, and V. Nistor, Biofabrication **7**, 35007 (2015).
12. J. Bueno, H. Ginis, R. Palacios, A. Pennos, and P. Artal, Invest. Ophthalmol. Vis. Sci. **54**, 5287 (2013).
13. K. Kuetemeyer, G. Kensah, M. Heidrich, H. Meyer, U. Martin, I. Gruh, and A. Heisterkamp, Opt. Express **19**, 15996 (2011).
14. D. Chai, T. Juhasz, D. J. Brown, and J. V. Jester, J. Biomed. Opt. **18**, 038003 (2013).
15. X. Chen, O. Nadiarynkh, S. Plotnikov, and P. J. Campagnola, Nat. Protoc. **7**, 654 (2012).
16. H. Y. Tan, Y. L. Chang, W. Lo, C. M. Hsueh, W. L. Chen, A. A. Ghazaryan, P. S. Hu, T. H. Young, S. J. Chen, and C. Y. Dong, J. Cataract Refract. Surg. **39**, 779 (2013).
17. J. P. Marquez, Int. J. Solids Struct. **43**, 6413 (2006).
18. J. M. Bueno, E. J. Gualda, A. Giakoumaki, P. Pérez-Merino, S. Marcos, and P. Artal, Investig. Opthalmology Vis. Sci. **52**, 5325 (2011).
19. R. McQuaid, J. Li, A. Cummings, M. Mrochen, and B. Vohnsen, Cornea **33**, 125 (2014).
20. J. M. Holopainen and K. Krootila, Am. J. Ophthalmol. **152**, 533 (2011).
21. P. Kamaev, M. D. Friedman, E. Sherr, and D. Muller, Investig. Ophthalmol. Vis. Sci. **53**, 2360 (2012).
22. A. Vogel, J. Noack, G. Hüttman, and G. Paltauf, Appl. Phys. B **81**, 1015 (2005).
23. G. Scarcelli, S. Besner, R. Pineda, P. Kalout, and S. H. Yun, JAMA Ophthalmol. **133**, 480 (2015).
24. G. Scarcelli, S. Kling, E. Quijano, R. Pineda, S. Marcos, and S. H. Yun, Investig. Ophthalmol. Vis. Sci. **54**, 1418 (2013).
25. G. Scarcelli, W. J. Polacheck, H. T. Nia, K. Patel, A. J. Grodzinsky, R. D. Kamm, and S. H. Yun, Nat. Methods **12**, 1132 (2015).
26. G. Scarcelli, S. Besner, R. Pineda, and S. H. Yun, Investig. Opthalmology Vis. Sci. **55**, 4490 (2014).
27. R. J. DeWall, Crit. Rev. Biomed. Eng. **41**, 1 (2013).
28. A. Manduca, T. E. Oliphant, M. a. Dresner, J. L. Mahowald, S. a. Kruse, E. Amromin, J. P. Felmlee, J. F. Greenleaf, and R. L. Ehman, Med. Image Anal. **5**, 237 (2001).
29. S. Wang and K. V. Larin, Biomed. Opt. Express **5**, 3807 (2014).
30. T. A. Planchon, L. Gao, D. E. Milkie, M. W. Davidson, J. A. Galbraith, C. G. Galbraith, and E. Betzig, Nat. Methods **8**, 417 (2011).
31. T. V. Truong, W. Supatto, D. S. Koos, J. M. Choi, and S. E. Fraser, Nat. Methods **8**, 757 (2011).
32. W. R. Zipfel, R. M. Williams, R. Christie, A. Y. Nikitin, B. T. Hyman, and W. W. Webb, Proc. Natl. Acad. Sci. USA **100**, 7075 (2003).
33. H. A. Collins, M. Khurana, E. H. Moriyama, A. Mariampillai, E. Dahlstedt, M. Balaz, M. K. Kuimova, M. Drobizhev, V. X. D. Yang, D. Phillips, A. Rebane, B. C. Wilson, and H. L. Anderson, Nat. Photonics **2**, 420 (2008).
34. Z. Meng, A. J. Traverso, and V. V. Yakovlev, Opt. Express **22**, 5410 (2014).

optica

Selective two-photon collagen crosslinking *in situ* measured by Brillouin microscopy: supplementary material

SHELDON J.J. KWOK,[1,2,3] IVAN A. KUZNETSOV,[1,3,4] MOONSEOK KIM[3], MYUNGHWAN CHOI[3,5,6], GIULIANO SCARCELLI[3,7], AND SEOK HYUN YUN[2,3,*]

[1]*These authors contributed equally*
[2]*Harvard-MIT Division of Health Sciences and Technology, 77 Massachusetts Avenue, Cambridge, MA 02139*
[3]*Wellman Center for Photomedicine, Massachusetts General Hospital, 50 Blossom Street, Boston MA 02114*
[4]*Department of Biomedical Engineering, Johns Hopkins University, 3400 North Charles Street, Baltimore MD 21218*
[5]*Department of Biomedical Engineering, Sungkyunkwan University, Suwon 16419, Korea*
[6]*Center for Neuroscience and Imaging Research, Institute for Basic Science (IBS), Suwon 16419, Korea*
[7]*Fischell Department of Bioengineering, University of Maryland, College Park, MD 20742*
**Corresponding author: syun@hms.harvard.edu*

Published 4 May 2016

This document provides supplementary information to "Selective two-photon collagen crosslinking measured by Brillouin microscopy", http://dx.doi.org/10.1364/optica.3.000469. The first section contains detailed information on the experimental methods, including sample preparation, crosslinking protocol, Brillouin measurements, and post-processing. The second section contains theoretical considerations, including comparison of laser parameters for one-photon and two-photon crosslinking, and calculation of the longitudinal modulus. The last section contains the supplementary figures cited in the manuscript.
http://dx.doi.org/10.1364/optica.3.000469.s001

1. MATERIALS & METHODS:

A. Corneal Preparation and Staining:

Fresh young bovine (<10 days) eyes were acquired and temporarily stored in ice-cold mineral oil to maintain hydration. After excess fat and optic nerve were removed from the eyes, the corneas were excised and stained with riboflavin according to the Dresden Protocol (epi-off), with the modification that the working riboflavin solution was 10% dextran w/v%, rather than 20%. The reason for this was that our preliminary results (data not shown) had determined that a 20% dextran riboflavin solution caused significant dehydration of the cornea, which introduced z-drift during the subsequent crosslinking and imaging steps. A 10% dextran solution prevented these unwanted effects. Note that the corneas were kept at 4° C during all steps of the above described procedure. Following staining, a central region of the cornea was removed using a 10 mm biopsy punch, mounted on a glass-slide, and gently compressed with a No. 1.5 coverslip for two-photon imaging and crosslinking.

B. Corneal Crosslinking:

For imaging and crosslinking, we used a home-built, video-rate, two-photon microscope. The system equipped a mode-locked Ti-Sapphire laser (MaiTai DeepSee eHP, Newport) as a light source which provides ~ 150 fs pulses at 80 MHz repetition rate. The scanning unit is composed of a polygon mirror for fast axis (x) and a galvanometer for slow axis (y), allowing frame rate of 30 Hz. Using a 20x, NA 0.9 water-immersion objective, the scanning area has dimensions of (290 x 480) μm^2. The emitted light was detected by photomuliplier tubes (PMT) through appropriate dichroic and bandpass filters. One PMT was used for detection of second harmonic generation (400 nm ± 5 nm) and another for riboflavin fluorescence (520 nm ± 35 nm).

Before imaging, the corneas were allowed to warm to room temperature to minimize temperature induced drift effects. Further XY-drift correction was implemented during post-processing in MATLAB. The top of the corneal stroma was determined by determining the Z-plane where SHG intensity abruptly changed. All depths are given relative to the top of the corneal stroma. To ensure that riboflavin had completely penetrated the cornea, a full Z-stack of a small XY-section of the cornea was first taken. 2P-CXL was performed at an average power of 104 mW, for 10 minutes per plane. To demonstrate three-dimensional, subsurface 2P-CXL, we crosslinked a vertically-aligned stack of 10 planes, equidistantly spaced 3 μm apart at depths of approximately -35 to -65 μm. The

crosslinking was monitored in real time and the riboflavin fluorescence and SHG intensity were recorded at 5 second intervals. If non-negligible drift was observed during this process, crosslinking was restarted with a different sample.

C. Brillouin Imaging:

The confocal Brillouin microscope is similar to previously described [1,2]. A single-mode, 532 nm, frequency-doubled Nd-YAG laser (Torus, Laser Quantum, Inc.) was used to illuminate the same with typical powers of 7 mW. A 10x, 0.3 NA air objective lens was used in the inverted, epi-illumination configuration. The scattered light was collected by a single-mode optical fiber, which also confers confocality, and delivers light to the high-resolution, apodized, two-stage VIPA spectrometer. Linearly variable intensity filters (Rugate and Newport 50FS04DV) were used for apodization. The diffracted light following the two-stage VIPA was detected with an EM-CCD camera with a dispersion slope of 0.3 GHz/pixel. The exposure time per pixel was 0.3 s. The image acquisition time varied from 0.5-2 hours, depending on the number of pixels. Calibration with reference materials was performed before each measurement as previously described.

Following crosslinking of a corneal sample, the XY location of the crosslinked region was marked on the glass slide with a marker and corneas were transferred to the Brillouin microscope. To minimize dehydration during imaging the corneas were submerged in mineral oil, and placed upside down on a glass-bottom dish for illumination from the bottom. The sample was translated in three-dimensions using a motorized stage (Prior Scientific, Inc.) with steps-sizes of 2-25 μm depending on the resolution required. The crosslinked region, as well as the surrounding areas, was thoroughly imaged by taking XY and XZ slices through the cornea.

D. Post-Processing:

To remove the PMT and laser-intensity noise from the collected two-photon microscope images, a combination of a median filter and a notch filter, respectively, were applied using custom-written MATLAB software. The filtered images were then analyzed for mean SHG, mean riboflavin intensity, and collagen fiber orientation. The fiber orientation was determined via a previously described protocol [3]. Briefly, edge detection and filtering were used to generate a binary mask of the collagen fibers from each SHG image. The inverse of this binary mask was multiplied with the original filtered image to suppress the non-collagen signal (Fig. S1). The FFT of the resultant image was taken and a bimodal Von Mises distribution was fit to the power in each radial angle of the output FFT. The mean of this distribution gave the average collagen fiber orientation in the image and the variance specified the alignment of the fibers.

The collected Brillouin data also required further processing. For each imaged voxel, the Brillouin microscope gives a spectral pattern consisting of the scattered light intensity as a function of Brillouin shift. This spectrum can be described by a Lorentz distribution with a mean equal to the characteristic Brillouin shift of the material. To determine the characteristic Brillouin shift of each voxel we used a least-squares error minimization methodology to fit a Lorentzian distribution to its output. A preliminary heat map of Brillouin shifts for each 2D Brillouin XY-slice was generated, and a 2D-median filter was applied to minimize noise. Using the corresponding Z location of each XY-slice, we then applied a 3D linear interpolation algorithm to generate a preliminary 3D view of the imaged Brillouin region. We then applied a 3x3x3 box kernel to generate the final 3D image. The relevant code was implemented in MATLAB.

2. THEORY

A. Comparison of laser parameters used for 1P and 2P-CXL

Here, we estimate the fluence and exposure time needed for 2P-CXL to match the laser parameters used for 1P-CXL with riboflavin and UVA light.

The number of excitations per molecule during the course of conventional one-photon CXL is expressed as follows:

$$N_{1p} = \frac{P * \sigma_{1p} * t}{A * h\nu_1} = 360\ \frac{excitations}{riboflavin\ molecule} \qquad \textbf{(S1)}$$

Here, A is the illuminated area, Power/Area (P/A) gives fluence, which is typically 3 mJ/(s*cm^2) at 365 nm, σ_{1p} is the 1P absorption cross-section of riboflavin which is 3.6x10^{-17}cm^2, t is 30 min, and $h\nu_1$ is the photon energy at 365 nm.

In contrast, the two-photon excitation rate depends on the spatial and temporal profile of the laser. We can express the total number of molecular excitations by integrating the intensity function squared over time and space, as follows:

$$N_{2p} = \frac{1}{2}\frac{\sigma_{2p}}{(h\nu_2)^2} * tflC \iiint_{-\infty}^{\infty} I^2(x,y,t)dxdydt \qquad \textbf{(S2)}$$

where the $1/2$ factor accounts for the two photons needed for two-photon absorption, tf represents the number of laser pulses within given time t, l is the optical path length, and C is the riboflavin concentration in molecules per unit volume.

Then the number of excitations per molecule is:

$$N_{2p} = \frac{1}{2}\frac{\sigma_{2p}}{(h\nu_2)^2} * \frac{tfl}{V} \iiint_{-\infty}^{\infty} I^2(x,y,t)dxdydt \qquad \textbf{(S3)}$$

where V is the excitation volume.

We can approximate the excitation volume divided by the optical path length to be equal to the 2P excitation area is approximated by the area of an ellipse: $A_{2p} = \pi\Delta x\Delta y$:

$$N_{2p} = \frac{1}{2}\frac{\sigma_{2p}}{(h\nu_2)^2} * \frac{tf}{\pi\Delta x\Delta y} \iiint I^2(x,y,t)dxdydt \qquad \textbf{(S4)}$$

Given Gaussian profiles for $I(x,y,t)$:

$$I(x,y,t) = I_0 * e^{-t^2/\tau^2} * e^{-x^2/(\Delta x)^2} * e^{-y^2/(\Delta y)^2} \qquad \textbf{(S5)}$$

Squaring and integrating over $x = -\Delta x$, $y = -\Delta y\ to\ \Delta y$, and $t = -\Delta\tau\ to\ \Delta\tau$, which correspond to the $1/e^2$ widths of the spatial and temporal profiles:

$$\iiint I^2(x,y,t)dxdydt = (I_0)^2 * (\frac{\pi}{2})^{\frac{3}{2}} * \tau\Delta x\Delta y * c \qquad \textbf{(S6)}$$

where c is a scaling factor equal to $\left[\frac{\int_{-1}^{1} e^{-2r^2}dr}{\int_{\infty}^{-\infty} e^{-2r^2}dr}\right]^3 \cong 0.87$

Equation S6 is in terms of peak irradiance (I_0). This can be expressed by an average power P_{avg} by the relation:

$$P_{avg} = f \iiint_{-\infty}^{\infty} I(x,y,t)dxdydt = \pi^{\frac{3}{2}} I_0 f\tau\Delta x\Delta y \qquad \textbf{(S7)}$$

where f is the repetition rate (Hz). Thus, we have:

$$(I_0)^2 = \frac{{P_{avg}}^2}{\tau^2 f^2} * \frac{1}{\pi^3} * \frac{1}{(\Delta x\Delta y)^2} \qquad \textbf{(S8)}$$

Combining Equations (S2-S8), we obtain:

$$N_{2p} \cong \frac{c}{4(2\pi)^{1/2}} * \frac{\sigma_{2p}}{(h\nu_2)^2} \frac{t}{\tau f} {P_{avg}}^2 \frac{1}{(A_{2p})^2} \quad \textbf{(S9)}$$

Here, σ_{2p} is 0.306 GM at 810 nm, τ is 150 fs , f is 80 MHz, while A_{2p} is calculated based on fitting of the illumination point spread function squared (IPSF²) to a Gaussian function. The $1/e^2$ radius (r_{2p}) of the IPSF² is expressed as [4]:

$$r_{2p} = \frac{0.325\,\lambda}{NA^{0.91}}, for\ NA > 0.7 \quad \textbf{(S10)}$$

where NA is the numerical aperture and **λ** is the wavelength of the incident radiation. For NA=0.9, we have r=0.29 μm, and $A_{2p} = \pi r^2 \cong 2.18 \times 10^{-9}$ cm².

Given an appropriate, non-toxic power (100 mW at 810 nm), and assuming $N = N_{2p} = N_{1p}$ we can solve for the exposure time needed:

$$t = \frac{4(2\pi)^{1/2}}{c} \frac{N(h\nu_2)^2 \tau f}{\sigma_{2p} {P_{avg}}^2} (A_{2p})^2 = 0.46\ ms \quad \textbf{(S11)}$$

The required fluence (F) for 2P-CXL is:

$$F = 0.46\ ms * \frac{100\ mW}{2.2x10^{-9} cm^2} = 2.1\ x\ 10^{-4}\ J/cm^2 \quad \textbf{(S12)}$$

Since 2P-CXL requires a focused beam which is scanned over a larger area, the illumination duty cycle must be taken into account to compute the practical exposure time, t'. For our system, A_{2p} is dispersed over a (290 x 480) μm² scanning area:

$$t' = t * \frac{Scanning\ area}{A_{2p}} = 4.9\ min \quad \textbf{(S13)}$$

B. Calculation of longitudinal modulus from Brillouin shift

Spontaneous Brillouin scattering occurs through photon-phonon interactions inside the material or tissue. The Brillouin shift (Ω) is given by [5]:

$$\Omega = 2K\sin(\frac{\theta}{2}) \sqrt{\frac{M'}{\rho}} \quad \textbf{(S14)}$$

where K is the photon wavenumber, Θ is the angle between incident and scattered photons, M' is the real part of the longitudinal modulus, and ρ is the mass density. We can see that the Brillouin shift is proportional to the propagation velocity $\sqrt{M'/\rho}$ of GHz acoustic waves inside the material.

For our epi-detection scheme, Θ = π, such that M' can be rewritten as:

$$M' = \frac{\rho\lambda^2\Omega^2}{4n^2} \quad \textbf{(S15)}$$

where λ is the wavelength of the incident light, and n is the refractive index. ρ/n^2 can be assumed to be approximately constant throughout the cornea at 0.56 g/cm³.

2. SUPPLEMENTARY FIGURES

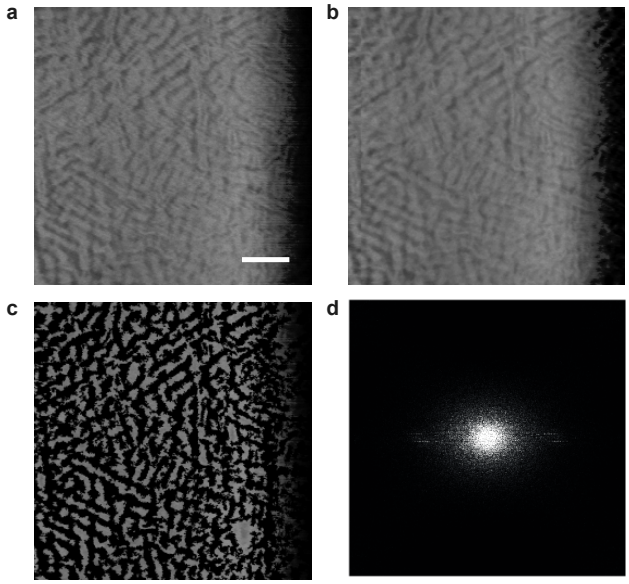

Supplementary Figure S1. (a) Raw SHG image of collagen fibers 50 μm below the cornea surface. (b) SHG image after median filtering of laser and PMT noise. (c) Image after edge detection and suppression of non-collagen signal. (d) 2D-FFT magnitude spectrum of c, which was used to quantify collagen fiber orientations. Scalebar: 50 μm.

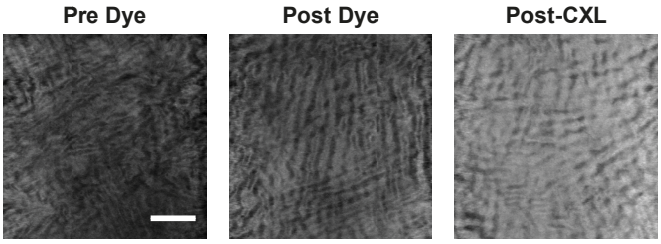

Supplementary Figure S2. Representative SHG images of bovince cornea pre and post application of riboflavin/dextran solution, as well as post 1P-CXL. Images shown are approximately 100 μm below the cornea surface. Scale bar: 50 μm

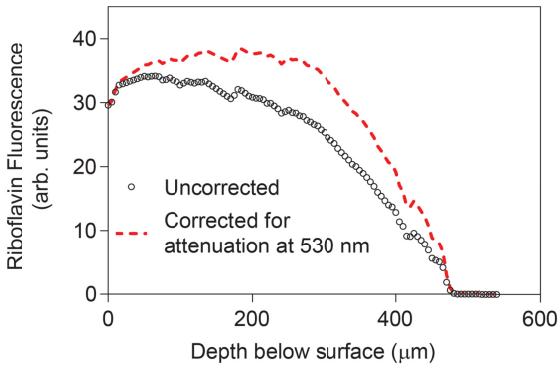

Supplementary Figure S3. Depth profile of riboflavin fluorescence prior to crosslinking. Red line is corrected for attenuation of collected light at 530 nm, assuming an attenuation coefficient of 10 cm^{-1}

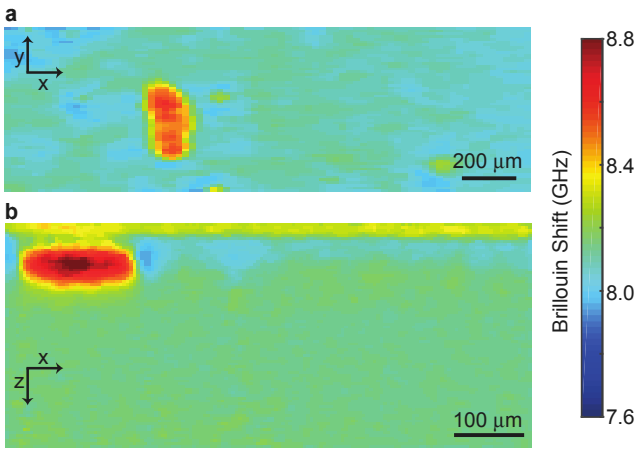

Supplementary Figure S4. (a) x-y image of 2P-CXL treated cornea, at 40 µm below the cornea surface. Step size: x=25 µm, y=10 µm. (b) x-z image of 2P-CXL treated cornea. Step size: x=5 µm, z=4 µm.

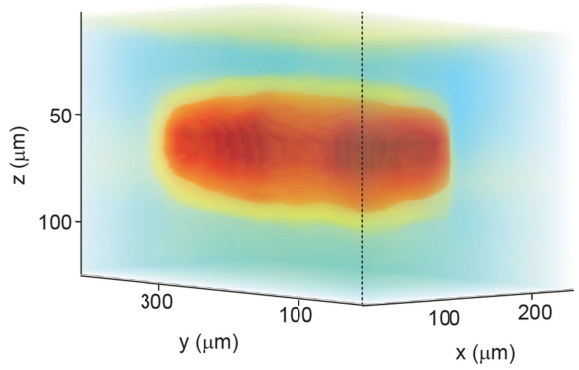

Visualization 1 (Movie File). Three-dimensional view of the 2P-CXL region reconstructed and interpolated from thirteen x-y images at 10 µm intervals in z. See Fig. 5.

REFERENCES:

1. G. Scarcelli, W. J. Polacheck, H. T. Nia, K. Patel, A. J. Grodzinsky, R. D. Kamm, and S. H. Yun, "Noncontact three-dimensional mapping of intracellular hydromechanical properties by Brillouin microscopy," Nat. Methods 1–5 (2015).
2. G. Scarcelli, S. Kling, E. Quijano, R. Pineda, S. Marcos, and S. H. Yun, "Brillouin microscopy of collagen crosslinking: Noncontact depth-dependent analysis of corneal elastic modulus," Investig. Ophthalmol. Vis. Sci. **54**, 1418–1425 (2013).
3. J. P. Marquez, "Fourier analysis and automated measurement of cell and fiber angular orientation distributions," Int. J. Solids Struct. **43**, 6413–6423 (2006).
4. W. R. Zipfel, R. M. Williams, and W. W. Webb, "Nonlinear magic: multiphoton microscopy in the biosciences.," Nat. Biotechnol. **21**, 1369–77 (2003).
5. J. M. Vaughan and J. T. Randall, "Brillouin scattering, density and elastic properties of the lens and cornea of the eye.," Nature **284**, 489–491 (1980).